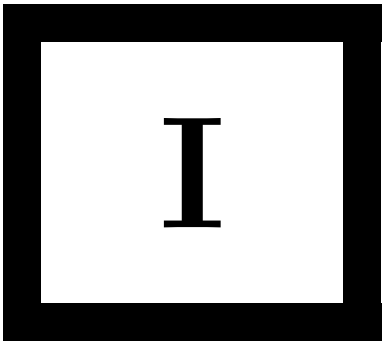

Publication I

J. Pulliainen, J-P. Kärnä, and M. Hallikainen. 1993. Development of geophysical retrieval algorithms for the MIMR. IEEE Transactions on Geoscience and Remote Sensing 31, no. 1, pages 268–277.

Development of Geophysical Retrieval Algorithms for the MIMR

Jouni Pulliainen, Juha-Petri Kärnä, and Martti Hallikainen, *Fellow, IEEE*

Abstract— **Results from a study concerning the feasibility of spaceborne microwave radiometry to retrieval of geophysical parameters are described. The study concentrates on the development of inversion techniques for multichannel spaceborne radiometers, especially the statistical inversion approach. The basic tool in this study was the developed simulation/inversion software. Especially, the applications of the planned MIMR instrument (Multi-Frequency Imaging Microwave Radiometer) are discussed. The employed inversion algorithms are 1) conventional algorithms for different applications and 2) the statistical inversion approach (maximum likelihood inverse solver). Comparisons between results from different inversion algorithms have also been carried out. The statistical inversion approach has been found to give promising parameter retrieval accuracies and is a potential tool to improve the operational use of passive spaceborne remote sensing. Additionally, sensitivity analysis of the radiometer apparent temperature to different geophysical parameters and the statistical behavior of the atmospheric transmissivity are presented.**

Keywords—**Spaceborne radiometry, passive microwave remote sensing, simulation software, inversion algorithm.**

I. Introduction

THE European Space Agency (ESA) develops the Multi-Frequency Imaging Microwave Radiometer (MIMR) for global research of the Earth's surface and atmosphere, scheduled for launch in the late 1990's. The MIMR will operate at six frequencies between 6.8 and 89 GHz, Table I [1]. The swath width is 1400 km, and the incidence angle is 50° off nadir. In order to fully employ the capabilities of the MIMR in Earth observation, dedicated inversion algorithms have to be developed.

The brightness temperature of a target depends on its physical temperature, surface geometry, and dielectric and extinction properties. Retrieval of a geophysical quantity from spaceborne radiometer data is possible if the effects of other parameters to the brightness temperature can be eliminated. When frequencies above 5 GHz are used, even the atmospheric effects have to be considered. In addition to target parameters, a variety of instrument parameters strongly affect the brightness temperature. These parameters include frequency, polarization, and angle of incidence.

Manuscript received November 31, 1991; revised April 22, 1992. This work was funded by the European Space Agency as part of the project "Study of Microwave Interaction with the Earth's Surface."

J. Pulliainen and M. Hallikainen are with the Helsinki University of Technology, Laboratory of Space Technology, Otakaari 5A, SF-02150, Espoo, Finland.

J.-P. Kärnä was with the Helsinki University of Technology. He is now with the Technical Research Centre of Finland.

IEEE Log Number 9204711.

TABLE I
MIMR Characteristics

Frequency (GHz)	Pixel size (km × km)	Accuracy (K)	Sensitivity (K)	Polarization
6.8	60 × 60	1.0	0.2	vertical, horizontal
10.65	38 × 38	1.0	0.4	vertical, horizontal
18.7	22 × 22	1.5	0.5	vertical, horizontal
23.8	20 × 20	1.5	0.5	vertical, horizontal
36.5	11.6 × 11.6	1.5	0.5	vertical, horizontal
89	4.9 × 4.9	1.5	0.7	vertical, horizontal

The main applications discussed in this paper are retrieval of 1) ocean surface parameters (sea surface temperature, wind speed, sea ice concentration), and 2) land parameters (snow extent, snow water equivalent, soil moisture). The retrieval methods are applicable to the MIMR. The main emphasis is on the statistical inversion approach, in which the inverse solution of the model representing the actual measurement is searched [2], [3]. The inverse solution is the one having the maximum likelihood of all the possible solutions.

II. Simulation of Emissivity

The basic equation for calculating the apparent temperature observed from space is

$$\begin{aligned} T_{a,p}(f,\theta) = {} & e_{s,p}(f,\theta)T_s t(f,\theta) + T_{a,\text{atmos}\uparrow} \\ & + T_{a,\text{atmos}\downarrow}\big(1 - e_{s,p}(f,\theta)\big)t(f,\theta) \\ & + 2.7\big(t(f,\theta)\big)^2\big(1 - e_{s,p}(f,\theta)\big) \end{aligned} \quad (1)$$

where

$e_{s,p}$ = surface emissivity,
T_s = temperature of the surface ,
$T_{a,\text{atmos}\uparrow}$ = up-welling atmospheric apparent temperature,
$T_{a,\text{atmos}\downarrow}$ = down-welling atmospheric apparent temperature,
t = transmissivity of atmosphere,
p = polarization,
θ = angle of incidence, and
f = frequency.

A simulation/inversion software of a spaceborne radiometer sensor is a system that a) calculates the apparent temperatures according to (1) at the instrument's frequencies of operation,

and b) employs specific inversion algorithms for the retrieval of geophysical parameters of interest. It can be utilized in the development and testing of inversion algorithms and, additionally, in the analysis of sensitivities of apparent temperatures for different geophysical parameters. Thus, a simulation/inversion software is a basic tool for the prelaunch evaluation of a spaceborne radiometer system.

The developed software simulates the microwave emission from the ocean, sea ice, snow-covered, and vegetation-covered land at the frequencies of the MIMR instrument. It uses theoretical, semi-empirical and empirical emission models.

A. Surface Emissivities

The following emission models were selected for the simulation of surface emissivity, $e_{s,p}(f,\theta)$ in (1):

- Pandey's model [4] for ocean surface,
- HUT (Helsinki University of Technology) model [5] for snow-covered land,
- Kerr's model [6] for vegetation-covered land,
- constant emissivity values for different ice types [7].

The current emission models for ocean surface work rather well in their specific validity area. The empirical Pandey's model was selected because of its simple mathematical formulation which makes it suitable for the statistical inversion method. The main restriction of the model, when compared, e.g., with Wilheit's model [8], is the frequency range of operation, which only extends up to 37 GHz.

Most snow models lack validation, due to difficulties in snow modeling, including 1) influence of numerous parameters on the microwave behavior of the snow layer, and 2) rapid changes of the values of these parameters with time and weather. The used emission model for snow is the semi-empirical HUT (Helsinki University of Technology) model which relies on experimental data from ground-based radiometer measurements with extensive ground truth. Kerr's semi-empirical model for vegetated land takes into account the effects of all relevant surface and vegetation layer (grass or corn) parameters. These parameters are: soil moisture, soil roughness, soil type, soil temperature, vegetation water content, vegetation albedo, canopy type, fractional coverage of vegetation, and vegetation effective temperature. The main limitation of the model is that it works well only up to 10 GHz. At higher frequencies the effect of surface roughness is not known. The dielectric constant of soil is calculated using the equations of Hallikainen *et al.* [9]. Additionally, the effect of forest canopy cover can be simulated by using surface emissivity correction coefficients that are based on experimental data [10].

None of the existing models, neither theoretical nor empirical, provide good accuracy for sea ice emissivity. Therefore, constant empirical values for the emissivity of different ice types are employed, Table II. The fundamental problem is the complex and relatively rapidly changing medium. Additionally, some of the physical parameters that have a major effect on the emissivity behavior, may vary considerably within the same ice type (locally or with time). Therefore, the behavior of parameters needed for sea ice microwave models is not well known. Especially, the statistical properties of the surface roughness and correlation length are almost totally uninvestigated. Presently, only the dielectric properties are known to some extent [11], [12].

TABLE II
ICE AND OPEN WATER EMISSIVITIES AT MIMR FREQUENCIES. DATA HAS BEEN GATHERED FROM SEVERAL SOURCES [7].

f/GHz	First-year ice	Multi-year ice	Open water
6.8 H	0.90	0.92	0.26
6.8 H	0.95	0.98	0.52
10.65 H	0.90	0.85	0.28
10.65 V	0.97	0.92	0.54
18.7 H	0.92	0.80	0.31
18.7 V	0.96	0.87	0.59
23.8 H	0.92	0.77	0.34
23.8 V	0.97	0.84	0.62
36.5 H	0.93	0.67	0.39
36.5 V	0.96	0.71	0.69
89.0 H	0.94	0.65	0.52
89.0 V	0.97	0.68	0.83

B. Atmospheric Emissivity and Transmissivity

Liebe's MPM [13], [14] model for the atmospheric absorption and extinction coefficients has been found to be the most suitable of the present microwave models to be used in the radiative transfer equation of the atmosphere [15]. It works well, especially at higher millimeter wave frequencies (up to 1000 GHz). The basic problem with all atmosphere models is validation. The current extinction and absorption coefficient models are semi-empirical, since the nature of continuum nonresonant absorption of gases is not fully understood [2].

Atmospheric emissivities and transmissivity, $T_{a,\mathrm{atmos}\uparrow}$, $T_{a,\mathrm{atmos}\downarrow}$ and $t(f,\theta)$ in Equation (1), are simulated by employing Liebe's model. Alternatively, the atmospheric parameters can be determined by using statistical transmissivity values. The following equations (2), (3), and (7)–(9) determine atmospheric emissivities and transmissivity when Liebe's model is employed, and (4)–(6) determine these parameters when statistical transmissivity values are used in the apparent temperature simulation.

The apparent temperature of the atmosphere seen from space at the altitude H is

$$T_{a,\mathrm{atmos}\uparrow}(H,\theta) = \sec\theta \int_0^H \kappa_a(z) T(z) e^{-\kappa_e(z,H)\sec\theta} dz \quad (2)$$

where κ_a is the absorption coefficient and $T(z)$ is the physical temperature of the atmosphere at height z. An analogous notation can be written for the down-welling temperature. The extinction term $\kappa_e(z,H)$ is

$$\kappa_e(z,H) = \int_z^H \kappa_e(z')dz' \quad (3)$$

The up-welling apparent temperature can also be written as

$$T_{a,atmos\uparrow} = \alpha_\uparrow T_s(1-t) \quad (4)$$

and an analogous notation can be written for the down-welling temperature. $\alpha_\uparrow$ is the approximate atmospheric profile factor

for determining the effective up-welling temperature $\alpha_\uparrow T_s$ of the atmosphere [16]:

$$\alpha_\uparrow = -0.073t^2 + 0.101t + 0.918. \quad (5)$$

Respectively, the profile factor for the downwelling temperature $\alpha_\downarrow T_s$ is [16]

$$\alpha_\downarrow = -0.035t^2 + 0.014t + 0.967. \quad (6)$$

The extinction coefficient κ_e is related to the transmissivity t by

$$t = e^{-\sec\theta \int_0^H \kappa_e(z)dz} \quad (7)$$

In order to calculate the absorption coefficients at different heights, the temperature and pressure profiles of the atmosphere are needed. The pressure profile used is [17]

$$p(z) = p_0 e^{-z/H_p} \quad (8)$$

where

p_0 = pressure at the ground level,
H_p = pressure scale height (7.7 km).

The temperature profile used in this paper is for the standard Finnish atmosphere. It is a linear model in which the atmosphere is divided into three layers. In the pressure and water vapor models the values of the scale height of the standard Finnish atmosphere are used. Similar models for atmospheric temperature and pressure profiles for different latitude zones can be found in Damosso *et al.* [18].

The density of water vapor is assumed to decrease exponentially with the scale height H_{wv} (2.35 km according to the standard Finnish atmosphere), as

$$\rho(z) = \rho_0 e^{-z/H_{wv}} \quad (9)$$

where ρ_0 is the ground level density.

The statistical values of the atmospheric transmissivity were retrieved from the propagation studies of Salonen *et al.* [15]. It gives the distribution of the atmospheric attenuation at 20, 30, 40, and 50 GHz. From these values the atmospheric transmissivities to be achieved for certain percentages of time have been calculated for the frequency band of 6 to 100 GHz using the Liebe's model, Fig. 1. The weather dependent statistical behavior of the apparent temperature is simulated by applying these values to (1) and (4)–(6).

An example of the program output of the emission calculation is in Fig. 2, which depicts a workstation screen during a program run. Separate lines represent different atmospheric transmissivities showing the effect of different atmospheric conditions. The effect of lower transmissivity on the higher frequency channels 4 (23.8 GHz), 5 (36.5 GHz), and 6 (89 GHz) can be clearly seen.

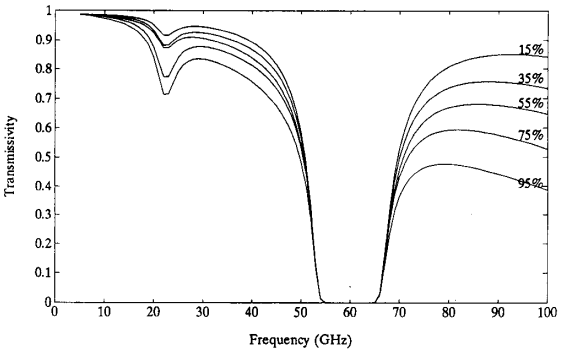

Fig. 1. Statistical behavior of the atmospheric transmissivity at 50° angle of incidence. The curves show the percentages of time when the transmissivity exceeds a certain value. The curves are calculated from data for southern Finland [15]. The data apply relatively well for northern latitudes (50–70°). An estimate for the water vapor content of 15% curve is 0.8 g/cm^2, for 55% curve 1.2 g/cm^2, and for 95% curve 3.3 g/cm^2.

III. Inversion Algorithms

A. Algorithms from Literature

Inversion algorithms for the above-mentioned atmospheric, ocean, snow, sea ice, and vegetation applications have been obtained from the literature. These algorithms are used in the developed simulation/inversion software, and their accuracy and confidence level have been tested. The algorithms are based on measurements or simulated data, using, e.g., the statistical multiple regression, and they are mathematically rather simple. The most usual forms are linear and logarithmic algorithms. Linear algorithms are valid if the atmospheric opacity is expected to be much less than one, i.e., the transmissivity value is near one. A logarithmic algorithm, in which the logarithm is taken from the subtraction of the apparent temperature and the surface temperature, takes the atmospheric conditions into account in a more advanced way [17]. Thus, it can be used for larger opacities.

The inversion algorithms implemented are:

- Miller's algorithm [19] for ocean surface wind speed,
- Wilheit's algorithm [20] for rain rate over the ocean,
- SPD algorithm [16] and Künzi's [21] algorithm for snow water equivalent,
- Swift's algorithm [22] for sea ice concentration,
- Lojou's algorithms [23], [24] for ocean surface temperature, and water vapor and liquid water content of atmosphere.

For soil moisture there are presently no advanced algorithms applicable to the MIMR. A low frequency channel (around 1.4 GHz) is desirable for soil moisture retrieval.

B. Statistical Inversion

Our development of inversion algorithms was concentrated on the so called statistical inversion approach (applied to the MIMR). The statistical inversion approach involves an algorithm based on the search of an inverse solution for the model representing the actual measurement [2], [3]. The used maximum likelihood inverse solver uses a nonlinear least-squares fitting method (Levenberg–Marquard) for fitting the model into the results of multichannel measurements. The minimizing problem is

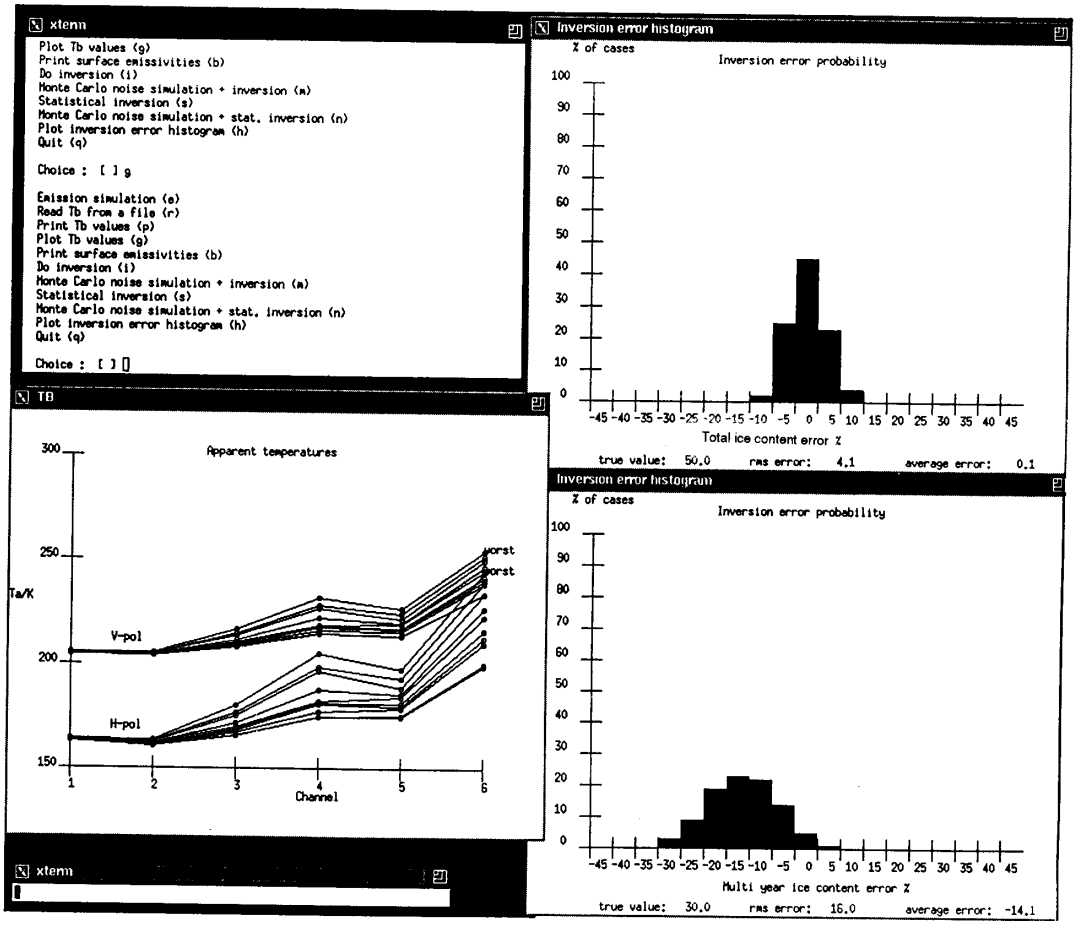

Fig. 2. Program screen showing emission calculation using statistical atmosphere and a subsequent inversion. Apparent temperatures are calculated for sea ice at horizontal and vertical polarizations using the statistical atmosphere model. On both polarizations there are ten separate apparent temperature vectors corresponding to ten separate atmosphere transmissivity conditions. The word "worst" denotes the lowest transmissivity condition.

$$\text{Minimize} \sum_{i=1}^{12} \frac{1}{2\sigma_i^2}(g_i(x_1, x_2, \ldots, x_n) - (T_a)_i)^2 + \sum_{j=1}^{n} \frac{1}{2\lambda_j^2}(x_j - \hat{x}_j)^2, \quad (10)$$

where

g_i = model representing the apparent temperature at the ith channel according to (1),
$(T_a)_i$ = apparent temperature at the ith channel, measured from space,
$x_1 \ldots x_n$ = model parameters, which include the geophysical parameters of interest,
$\hat{x}_j$ = average value of the jth model parameter (*a priori* information),
λ_j = standard deviation of the jth model parameter value, and
σ = standard deviation of (Gaussian) measurement noise.

The initial values for the model parameters, $x_1, x_2, \ldots, x_n$, are obtained from previously mentioned inversion algorithms or, in case no algorithm exists, they are set to default values (expected values according to *a priori* information). It is also possible to use absolute limits for certain model parameters, e.g., wind speed ≥ 0 m/s, etc.

The developed technique is a unified method for retrieval of the geophysical parameters of any surface type. The algorithm solves a parameter set containing all the parameters relevant for the apparent temperature measured from space. The surface emissivity is defined by empirical or theoretical emission models (see Section II). The method allows the utilization of *a priori* information on any parameter related to the radiometer measurement. The additional sum term in (10) takes into account *a priori* information on a Gaussian distributed parameter.

For the atmospheric transmissivity, a statistical principal component model is utilized. This model was developed for the MIMR frequencies by employing the curves of Fig. 1. The principal component model allows the reduction of the

TABLE III
PRINCIPAL COMPONENTS OF ATMOSPHERIC TRANSMISSIVITY

Freq. (GHz)	6.8	10.65	18.7	23.8	36.5	89
t_P^0	0.9851	0.9795	0.9390	0.8637	0.8731	0.6813
t_P^1	0.0088	0.0275	0.1582	0.3851	0.2652	0.8692
t_P^2	0.0178	0.0124	−0.2456	−0.8753	0.0733	0.4096

statistical atmospheric transmissivity behavior in the model representing the measurement into only one free parameter (a six-component vector according to six frequencies of the MIMR). Thus, (10) can be expressed (when *a priori* information is excluded for convenience) as

$$\text{Minimize} \sum_{i=1}^{12} \frac{1}{2\sigma_i^2}\left(g_i(x_1,\ldots,x_n,\alpha,\gamma^1) - (T_a)_i\right)^2 \quad (11)$$

where

α = atmospheric profile factor that contains information about the pressure, water content, etc. of the atmosphere; and

γ^1 = scalar variable (value of the first atmospheric transmissivity principal component).

The factor α is assumed to be the same in both upward and downward direction, which is a fair approximation (refer to (5) and (6)). According to (1) the emission model g may be written

$$\begin{aligned} g_i(x_1,\ldots,x_n,\alpha,\gamma^1) &= e_i(x_1,\ldots,x_n)T_s t_k(\gamma^1) \\ &\quad + \alpha T_s\left(1 - t_k(\gamma^1)\right) \\ &\quad + \alpha T_s(1 - e_i(x_1,\ldots,x_n))t_k(\gamma^1)\left(1 - t_k(\gamma^1)\right) \\ &\quad + 2.7(1 - e_i(x_1,\ldots,x_n))t_k(\gamma^1)^2 \end{aligned} \quad (12)$$

where t_k is the atmospheric transmissivity at the kth frequency obtained by the statistical principal component model:

$$t_k(\gamma^1) = t_{P_k}^0 + \gamma^1 t_{P_k}^1, \qquad k = 1\ldots6 \quad (13)$$

where

t_P^0 = average atmospheric transmissivity vector (average values at the six MIMR frequencies),

γ^1 = a scalar variable and

t_P^1 = the first principal component of the atmospheric transmissivity vector:

$$t_P^1 = \left(t_{P_1}^1 t_{P_2}^2 \ \ldots\ t_{P_6}^1\right)^T. \quad (14)$$

The principal components of the atmospheric transmissivity have been retrieved by principal component regression for the transmissivity values of Fig. 1 [25], [2]. The basic idea is to find the orthonormal system optimally in the sense that only the first few components are needed to approximate the atmospheric transmissivity behavior satisfactorily in the square mean sense (the first one is sufficient in this case). Table III gives the obtained atmospheric transmissivity components t_P^0, t_P^1 and, additionally, the second principal component t_P^2 for southern Finland.

IV. SOFTWARE IMPLEMENTATION

The software was implemented in the UNIX environment using C language and X Window System for the graphics output. The software was also ported to MS-DOS environment.

The software includes emission simulation and inversion modules. The emission calculation can also be entirely skipped by reading the apparent temperature values from a file in order to use measured data. The inversion module employs either conventional algorithms or the statistical inversion. In the statistical inversion, Levenberg–Marquard method [26] is used for solving the minimizing problem.

The software allows one to investigate the sensitivity of the inversion algorithms to the system noise by using the Monte Carlo noise simulation. In this method random noise is added to the apparent temperature values, after which inversion is performed.

Fig. 2 depicts a snapshot of the workstation screen which has windows showing the apparent temperature values and inversion result histograms.

The user can change both the frequencies and the number of channels in order to use the software for simulating other radiometers as well, keeping in mind the validity area of the emission models and inversion algorithms.

V. SENSITIVITY OF THE APPARENT TEMPERATURE TO GEOPHYSICAL PARAMETERS

A. Mathematical Basis for Sensitivity Analysis

Sensitivity analysis of the apparent temperature reveals the quantitative effects of different parameters affecting the measurement, i.e., the effects of the parameters of interest and the disturbing parameters. Therefore, it is an essential part of developing inversion techniques and necessary for the selection of instrument characteristics. Sensitivity is defined as

$$S = \frac{\partial T_a}{\partial x} \quad (15)$$

where T_a is the apparent temperature and x is an affecting parameter.

The sensitivity analysis discussed below was performed by using (1) to (9). The microwave parameters e_s and t in (1) and (4)–(6) were determined from the models and statistical transmissivity data discussed in Section II. Additionally, the exact radiative transfer model given in (2) and (3), and a similar formula for the down-welling temperature, both applied to (1), were employed.

B. Examples of Results

The sensitivity of the apparent temperature to the near surface wind speed (at the height of 20 m above sea level, incidence angle 50°) is illustrated in Fig. 3. The sensitivity is obtained from

$$\frac{dT_a}{dW} = \frac{de_s}{dW}\left(T_s t - \alpha_\downarrow T_s(1-t)t - 2.7t^2\right) \quad (16)$$

where W is the wind speed. The surface emissivity e_s is a function of wind speed and is given by Pandey's model [4].

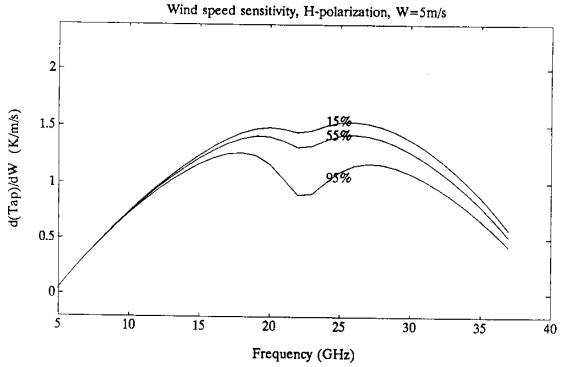

Fig. 3. Sensitivity of the satellite observed apparent temperature to the ocean surface wind speed at the wind speed of 5 m/s. The surface temperature is 15°C. The curves show the fraction of time when the sensitivity exceeds a certain value.

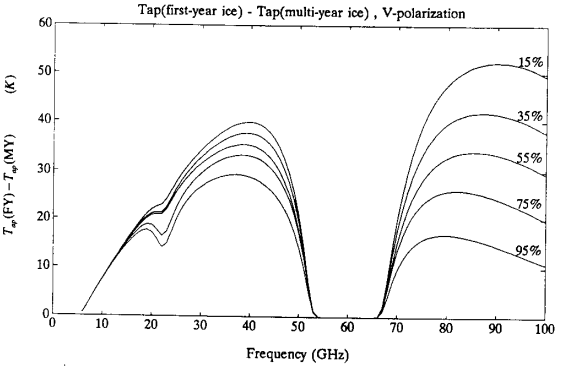

Fig. 4. The difference of the satellite observed apparent temperature between first-year ice and multiyear ice at vertical polarization. Angle of incidence is 50°. The curves show the fraction of time when the sensitivity exceeds a certain value. The apparent temperatures are determined by (1) using discrete sea ice emissivity values. The emissivity values at other frequencies are approximated by a second degree polynomial fit.

The results are shown for three transmissivities exceeded 15%, 55%, and 95% of time. The results show clearly the increasing effect of atmospheric disturbance when the frequency exceeds 15 GHz and thus the application of the four highest MIMR frequencies for determining the wind speed becomes questionable. The transmissivity values, used in the analysis, apply to northern latitudes (50–70°) [15].

A similar approach has been used in Fig. 4, which shows the change of the apparent temperature when the observed surface changes from multiyear ice to first-year ice. The emissivities used for the ice types are depicted in Table II. The figure indicates the potential capability of the 89 GHz channels for distinguishing multiyear ice from first-year ice. However, the graphs also demonstrate that in order to acquire reliable results at 89 GHz the atmospheric effects should be properly eliminated.

The sensitivity of the apparent temperature to the grain size is presented in Fig. 5. The sensitivity (S_d , [K/mm]) is calculated using the HUT snow model and the following

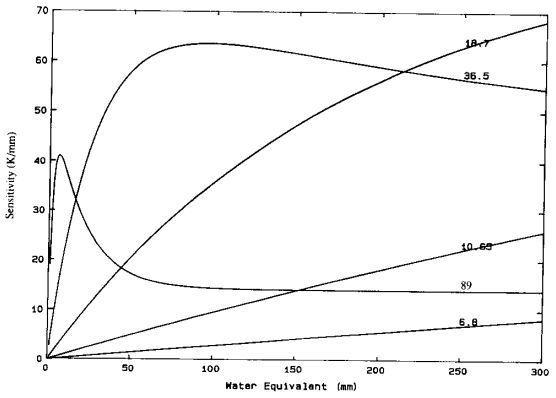

Fig. 5. Sensitivity of the satellite observed apparent temperature to the snow grain size as a function of snow water equivalent. The curves are calculated at the MIMR frequencies relevant for snow applications, and using vertical polarization. The behavior at horizontal polarization is similar.

equation:

$$S_d = -\frac{T_a(d = 0.4\text{mm}) - T_a(d = 1.2\text{mm})}{(0.4 - 1.2)\text{mm}} \tag{17}$$

The following assumptions are used in the calculations:

- emissivities of ground at different frequencies are those presented in [24] for frozen ground
- temperature of ground = −1°C
- grain diameter d = 0.8 mm
- density of snow = 0.24 g/cm^3
- snow surface roughness = 0.0 mm
- no vegetation is present
- the transmissivity and the brightness temperature of the atmosphere have been calculated using Liebe's model for (2) and (3). The standard atmosphere measured at Jokioinen in southern Finland in January and the following surface parameters are used:
  - pressure = 1013 mbar
  - temperature = −5°C
  - humidity = 80%.

The results for snow show the strong dependence of the apparent temperature to the grain size at 18.7 GHz, 36.5 GHz and also at 89 GHz (when the water equivalent is smaller than 20 mm). The high sensitivity deteriorates the accuracy of snow water equivalent retrieval when the grain size cannot be estimated properly. The results also indicate the potential of the 89 GHz channels for determining the snow extent. Recent experimental results on SSM/I 85 GHz channel are encouraging [27].

C. Summary of the Sensitivities

Table IV summarizes the quantitative effects of different surface parameters to the apparent temperature observed by a spaceborne sensor. The table shows the change of the apparent temperature caused by a change in a single parameter value. The other parameters remain constant (same as those used in Figs. 3–5). The used parameter value ranges are close

TABLE IV
OVERVIEW OF THE SENSITIVITY OF THE APPARENT TEMPERATURE TO DIFFERENT SURFACE PARAMETERS AND THE ATMOSPHERIC TRANSMISSIVITY

Parameter and range	Change of apparent temperature ΔT_a						
	Frequency (GHz)						
	Polarization	6.8	10.65	18.7	23.8	36.5	90.0
Ocean surface wind speed 5-7 m/s	Horizontal	W	W	M	M	W	-
	Vertical	W	W	W	W	W	-
Ocean surface temperature 18-20°C	Horizontal	W	W	M	M	M	-
	Vertical	W	W	M	M	W	-
Atmospheric transmissivity 15-95%	Horizontal	W	M	S	S	S	-
	Vertical	W	M	S	S	S	-
Total ice concentration 50-52%	Horizontal	M	M	M	M	M	W
	Vertical	M	M	W	W	W	W
Multiyear ice fraction 80-85%	Horizontal	W	W	W	W	M	S
	Vertical	W	W	W	W	M	M
Atmospheric transmissivity 15-95%	Horizontal	W	W	M/S	S	S	S
	Vertical	W	W	M	S	S	S
Snow water equivalent 10-15mm	Horizontal	W	W	W	M	S	M
	Vertical	W	W	W	M	S	M
Atmospheric transmissivity 15-95%	Horizontal	W	W	M	M	M	S
	Vertical	W	W	W	M	M	S

W = weak: $\Delta T_a < 2K$,
M = moderate: $2K \leq \Delta T_a < 8K$,
S = strong: $\Delta T_a \geq 8K$.

to retrieval accuracies required by end users. The apparent temperature changes are divided into three categories: weak (change is smaller than 2K), moderate (between 2K and 8K) and strong (more than 8K). For comparison, the magnitude of atmospheric disturbance is presented. The disturbance level is the change of the apparent temperature caused by the change of the atmospheric transmissivity value from the value exceeded 95% of time to the value exceeded 15% of time (see Fig. 1). Comparison of atmospheric disturbance level with the sensitivity to each target parameter in Table IV shows that in several cases atmospheric effects are stronger than the effects of the target parameters.

VI. COMPARISON OF INVERSION ALGORITHMS

The evaluated inversion algorithms include (1) the statistical inversion approach and (2) the conventional algorithms described in Section III.

The apparent temperatures at MIMR channels have been simulated by the developed simulation/inversion software. For the surface parameter algorithm testing the simulations have been carried out using both 1) precisely defined average atmospheric conditions (and Liebe's model); and 2) statistical atmosphere parameters according to Fig. 1. Table V shows

TABLE V
COMPARISON OF ACCURACY OF CONVENTIONAL ALGORITHMS AND THE STATISTICAL INVERSION APPROACH. THE TEST RUN RESULTS SHOW THE ERROR RANGES UNDER VARYING SURFACE AND ATMOSPHERIC PARAMETER CONDITIONS (FOR ATMOSPHERIC TRANSMISSIVITY, THE VALUES PRESENTED IN FIG. 1 WERE UTILIZED). THE NOISE LEVEL IN SIMULATIONS WAS 1 K. REPORTED TYPICAL RETRIEVAL ACCURACIES FOR SPACEBORNE DATA ARE ALSO PRESENTED.

Application	rms error	
	Conventional algorithm	Statistical inversion
Ocean surface wind speed [m/s]	1 - 6 (Miller) <2 (*)	1
Ocean surface temperature [°C]	2 - 10 (Lojou) >1 (**)	1 - 2
(*) Reported accuracy for the SSM/I algorithm of Goodberlet et al. under typical conditions (achievable for 85% of time) [28]. (**) Reported accuracies for Wilheit's and Wentz's algorithms [20,29,30].		
Total ice concentration [%]	2 - 10 (Swift) <4 (*)	0 - 5
Multiyear ice concentration [%]	10 - 35 (Swift) 10 - 20 (*)	3 - 30
(*) Typical values from Swift's algorithm according to [7].		
Snow water equivalent [mm]	10 - 50 (SPD)	5 - 50 (*) 10 - 80
(*) With *a priori* information.		

TABLE VI
RMS ERRORS OF THE TOTAL ICE CONCENTRATION PERCENTAGES, OBTAINED WITH THE STATISTICAL INVERSION APPROACH APPLIED TO THE MIMR. THE EMISSIVITIES OF THE DIFFERENT ICE TYPES HAD A $\pm$ 0.1 RANDOM ERROR UNIFORMLY DISTRIBUTED AROUND THE VALUES USED IN THE INVERSE SOLVER. (FY = FIRST-YEAR ICE FRACTION [%], MY = MULTIYEAR ICE FRACTION [%].)

FY (%) / MY (%)	0	20	40	60	80	100
0	0	1	2	4	3	4
20	1	2	3	3	3	-
30	2	3	2	3	-	-
60	2	4	4	-	-	-
80	3	2	-	-	-	-
100	5	-	-	-	-	-

the comparison of statistical inversion approach against the conventional algorithms. The retrieval accuracies with conventional algorithms are based on test runs and values reported in the literature. The values presented in Table V were achieved by test runs under different atmospheric and surface parameter conditions. An example of a test run set providing values to Table V is presented in Table VI. In the test runs of statistical inversion no *a priori* information, (19), were utilized, except in the case of snow-covered terrain.

In the conducted test runs, the wind speed and surface temperature retrieval accuracies of statistical inversion method have been found to be better or equal to those from conventional algorithms (see Table V and the values presented in Figs. 6 and 7 at 1 K noise level). The wind speed range in

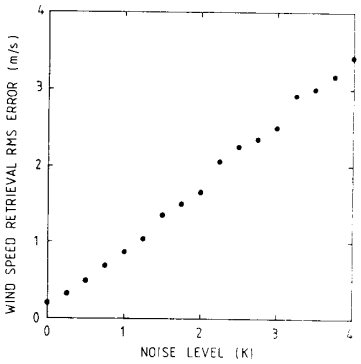

Fig. 6. Effect of Gaussian noise to retrieval accuracy of wind speed (statistical inversion approach).

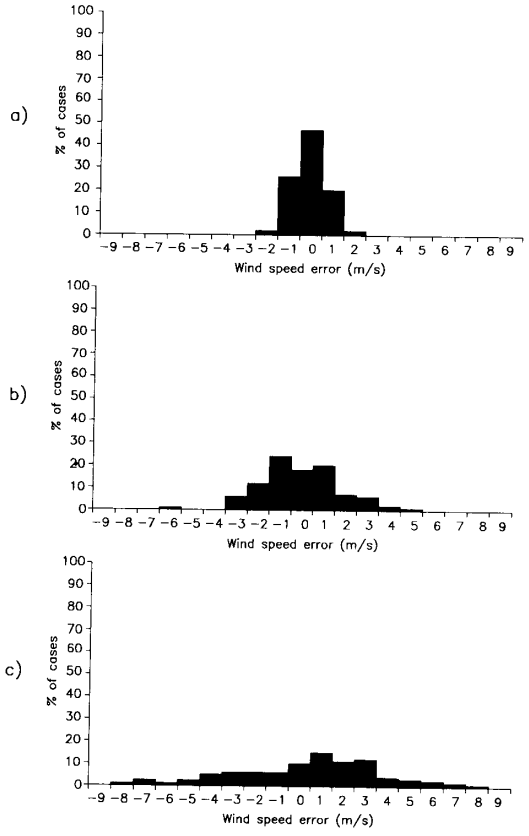

Fig. 7. Inversion error distributions for wind speed retrieval (statistical inversion approach) at different levels of Gaussian noise. The distributions are determined by Monte Carlo noise simulation. a) Noise deviation 1 K. b) Noise deviation 2.5 K. c) Noise deviation 4 K.

the test runs was from 0 to 20 m/s, and the temperature range was from 0 to 20°C.

Swift's algorithm appears to be the most suitable conventional algorithm for mapping ice type concentration [7]. The conclusion from the comparison between Swift's algorithm and the statistical inversion approach is that the statistical method seems to be more accurate for sea ice applications (Table V). See also Table VI for total ice concentration retrieval error distribution for statistical inversion approach under different conditions. However, comparison and testing of the algorithms using experimental data with proper ground truth data is needed. These data can be obtained with airborne or spaceborne instruments.

The two conventional algorithms, SPD and Künzi's algorithms [16], [21], gave relatively good retrieval results in the conducted test runs for snow water equivalent retrieval, the smallest rms errors being about 10 mm (Table V). However, this accuracy is not realistic for satellite-borne measurements, mainly due to the poor spatial resolution of a spaceborne instrument. Test runs of the statistical inversion approach were carried out both using and without using a priori information on grain size (diameter mean values with 0.2 mm maximum offset and 0.2 mm standard deviation, (19)). The following conclusions can be drawn from the test run results of the statistical inversion approach applied to snow cover:

1) With appropriate *a priori* information the statistical approach gives good accuracy (better than the conventional algorithms).
2) If no *a priori* information is available or if *a priori* information is not accurate enough, the statistical approach may give poor results.

The snow water equivalent range used in test runs was from 25 to 100 mm. This corresponds to regular snow conditions in southern Finland.

The statistical inversion approach was the only available method to be used for vegetated land. Its basic problem is the large number of parameters involved in the emission behavior. Especially, the effect of the soil surface roughness tends to handicap the determination of soil moisture. The effect of other parameters is smaller, since errors in the vegetation water content and vegetation cover fraction may compensate each other, and effects of clay and sand content fractions are minimal. Therefore, prior information on the surface roughness should be available in order to get reliable estimates for the soil moisture.

A. Conclusions on the Statistical Inversion Approach

The used statistical inversion method gives accurate estimates when the number of parameters contributing to the emission behavior is small (see (10)–(12)). When the parameter set is large the method may give poor results. In practice, vegetated or snow-covered land belongs to the latter class, whereas ocean and ice-covered sea belong to the former category.

In ocean and sea ice applications the number of model parameters is 2 or 3, plus one atmosphere parameter γ^1 (atmospheric profile factor α of (12) has been set to a constant value). The parameters for open sea are wind speed and temperature (the effect of salinity is negligible) and for sea ice they are temperature, total ice concentration, and multiyear ice fraction. The conducted test runs show that in this case the statistical method gives more accurate results than the conventional methods.

In land applications the number of important surface parameters is 6 to 8. For snow-covered terrain they include snow water equivalent, snow density, grain size, snow temperature, surface roughness, and forest cover fraction (and forest type). For snow-free terrain they include soil moisture, soil temperature, canopy cover fraction, vegetation water content, vegetation temperature, and surface roughness. Most of these parameters are variables to be determined with the algorithm, and some of them are treated with constant default values. The test runs indicate that a large number of affecting parameters decreases the accuracy of the method. However, if statistical *a priori* information on the parameters is available, the statistical approach works better. Furthermore, if studies concerning the (statistical) relations of different effective parameters were undertaken, the number of parameters could be reduced, and thus, the accuracy would increase.

The effect of measurement noise to the statistical inversion algorithm is demonstrated in Figs. 6 and 7. These figures are calculated for the case of wind speed retrieval, but the behavior is similar also for other applications. The figures imply that the sensitivity of statistical inversion to the Gaussian measurement noise is not drastic with the practical measurement accuracies of spaceborne sensors. This is an expected result, since all the channels sensitive to different geophysical parameters are employed.

The benefits of the used statistical inversion method, and the aspects that make it a unified inversion technique are the following:

- It can be used for any application area (if there is a modeling approach for the measurements: theoretical, empirical or statistical).
- It can be used with any set of channels (polarizations or frequencies).
- Multiple instrument approach can be adopted easily.
- Statistical *a priori* information can be employed.
- Range limits for parameter values can be easily set.
- Atmospheric effects (disturbances) have been reduced into one free parameter (by a statistical principal component model), which increases the method's reliability of resolving the surface parameters of interest.

The major limitations of the used statistical inversion system include the following viewpoints:

- The current system was not implemented for atmospheric applications.
- In land surface applications the number of important parameters is large and their statistical behavior is poorly known; the same applies to the relations between the individual parameters. Thus, the applicability of the current system for land surfaces is relatively poor.
- Misleading *a priori* information (wrong mean value of a parameter assumed to be known) may cause a large error, refer to rms error values for snow given in Table V.

VII. Conclusions

The performed sensitivity analysis of the apparent temperature implies the potential of the 89 GHz channels of the MIMR especially for improving discrimination of first-year ice from multiyear ice. That frequency can also be beneficial for snow applications, especially for eliminating grain size effects and detecting shallow snow. Additionally, our sensitivity analysis shows the atmospheric disturbance levels for different applications and their statistical distributions. These aspects have been taken into account insufficiently in most of the present inversion algorithms. The statistical distributions were determined using the transmissivity statistics obtained for conditions of southern Finland.

The development and testing of inversion algorithms (all applicable for the MIMR) was concentrated on a unified statistical inversion approach. An advantage of this approach is the use of all measured information at various channels. A novel feature of our algorithm is the reduction of the number of atmospheric parameters with a statistical model developed for the MIMR frequencies. This improves the accuracy of the method, since the number of affecting parameters is a critical factor. The statistical inversion approach has been shown to be promising particularly for ocean and sea ice applications. For land applications the accuracies needed by the end users are difficult to obtain with the statistical approach as well as with the conventional algorithms. That is mainly due to the large number of parameters influencing the emission behavior.

Acknowledgment

The ESA technical management of the project has been under Maurice Borgeaud. The authors wish also thank Ville Jääskeläinen for Fig. 5 and Erkki Somersalo for his contribution in the development of the statistical inversion approach.

References

[1] Y. Menard and M. Reynolds, "The design of the ESA Multiband Imaging Microwave Radiometer MIMR," *IEEE 1991 Int. Geosci. Remote Sensing Symposium (IGARSS'91)*, pp. 2359–2363, June 3–6, 1991.

[2] J. Pulliainen, M. Hallikainen, E. Somersalo, J.-P. Kärnä, V. Jääskeläinen, J. Hyyppä, J. Talvela, J.-P. Luntama, and T. Manninen, *Study of Microwave Interaction with the Earth's Surface, Final Report Vol. 1: Passive Microwave Remote Sensing.* Study under ESTEC Contract 8447/89/NL/PB(SC), 371 pp., 1990.

[3] M. Lehtinen, "On statistical inversion theory," *Theory and Applications of Inverse Problems* (Pitman Research Notes in Mathematics Series 167), pp. 46–57, 1988.

[4] R. Pandey and K. Kakar, "An empirical microwave emissivity model for a foam-covered sea," *IEEE J. Geophys. Res.*, vol. 79, pp. 135–140, 1982.

[5] M. Hallikainen, V. Jääskeläinen, and J. Talvela, "Results from ground-based radiometry of snow," *IEEE 1989 Int. Geosci. Remote Sensing Symposium (IGARSS'89)* (Vancouver), pp. 1231–1234, July 10–14, 1989.

[6] Y. Kerr and E. Njoku, "A semi-empirical model for interpreting microwave emission from semiarid land surfaces as seen from space," *IEEE Trans. Geosci. Remote Sensing*, vol. 28, pp. 384–393, 1990.

[7] P. Gudmandsen, "Sea ice retrieval algorithm studies (appendix F.2)," *Study of Microwave Interaction with the Earth's Surface*, Study under ESTEC Contract 8328/89/NL/PB(SC), pp. 247–273, 1990.

[8] T. Wilheit, "A model for the microwave emissivity of the ocean's surface as a function of wind speed," *IEEE Trans. Geosci. Electronics*, vol. GE-17, pp. 244–249, 1979.

[9] M. Hallikainen, F. Ulaby, M. Dobson, M. El-Rayes, and L. Wu, "Microwave dielectric behavior of wet soil - Part 1: Empirical models and experimental observations," *IEEE Trans. Geosci. Remote Sensing*, vol. GE-23, pp. 25–34, 1985.

[10] V. Jääskeläinen and M. Hallikainen, "Analysis of brightness temperature of snow-covered terrain," *IEEE 1991 Int. Geosci. Remote Sensing Symposium (IGARSS'91)* (Helsinki), pp. 2323–2327, June 1991.

[11] M. Vant, R. Ramseier, and V. Makios, "The complex-dielectric constant of sea ice at frequencies in the range 0.1–40 GHz," *J. Appl. Phys.*, vol. 49, pp. 1264–1280, 1978.
[12] M. Hallikainen, "Review of the microwave dielectric and extinction properties of sea ice and snow," *IEEE 1992 Int. Geosci. Remote Sensing Symposium (IGARSS'92)* (Houston), pp. 961–965, May 26–29, 1992.
[13] H. Liebe, "MPM - an atmospheric millimeter-wave propagation model," *Int. J. Infrared and Millimeter Waves*, vol. 10, pp. 631–650, 1989.
[14] H. Liebe, "Atmospheric attenuation and delay rates between 1 GHz and 1 THz," Conference on Microwave Propagation in the Marine Boundary Layer, Monterey, CA, USA, Sept. 1988.
[15] E. Salonen, S. Karhu, P. Jokela, S. Uppala, S. Sarkkula, and H. Aulamo, "Study of propagation phenomena for low availabilities.," Final Report under ESTEC Contract 8025/88/NL/PR, pp. 193–244, 1990.
[16] J. Aschbacher, "Land surface studies and atmospheric effects by satellite microwave radiometry," Ph.D. dissertation, University of Innsbruck, 1989.
[17] F. Ulaby, R. Moore, and A Fung, *Microwave Remote Sensing, Vol. I: Microwave Remote Sensing Fundamentals and Radiometry*. Addison-Wesley Publishing Company, 1981.
[18] E. Damosso, L. Stola, and G. Brussaard, "Characterisation of the 50–70 GHz band for space communications," *ESA Journal*, vol. 7, 1983.
[19] R. Miller, J. Geyser, A. Chang, and T. Wilheit, "Observations of oceanic surface-wind fields from the Nimbus-7 microwave radiometer," *IEEE Trans. Geosci. Remote Sensing*, vol. GE-20, pp. 550–554, 1982.
[20] T. Wilheit, "Retrieval of ocean surface parameters from the SMMR on the Nimbus-7 satellite," *IEEE Trans. Geosci. Remote Sensing*, vol. GE-22, pp. 133–143, 1984.
[21] K. Künzi, S. Patil, and H. Rott, "Snow-cover parameter retrieval from Nimbus-7 Scanning Multichannel Microwave Radiometer (SMMR) data," *IEEE Trans. Geosci. Remote Sensing*, vol. GE-20, pp. 452–467, 1982.
[22] C. Swift, I. Fedor, and R. Ramseier, "An algorithm to measure sea ice concentration with microwave radiometers," *J. Geophys. Res.*, vol. 90, pp. 1097–1099, 1985.
[23] R. Bernard, C. Klapisz, and J.-Y. Lojou, *Algorithms for Atmospheric and Sea Surface Observation Applications to MIMR*. Subcontractor Report under ESTEC Contract 8447/89/NL/PB(SC) Study of Microwave Interaction with the Earth's Surface, 1990.
[24] J.-Y. Lojou, "Algorithmie et Methodes de Validation des Instruments en Radiometrie Hyperfrequence," Ph.D. dissertation (in French), University of Paris 7, 1990.
[25] T. Anderson, *An Introduction to Multivariate Statistical Analysis* (2nd ed.). New York: Wiley & Sons, 1984 .
[26] H. Press, B. Flannery, S. Teukolsky, and W. Vetterling, *Numerical Recipes in C*. Cambridge, England: Cambridge University Press, 1988.
[27] H. Rott., T. Nagler, and J. Aschbacher, "Algorithm developments for monitoring the global snow cover by spaceborne microwave radiometry," 11th EARsel Symposium (Graz, Austria), pp. 58–69, 1991.
[28] M. Goodberlet, C. Swift, and J. Wilkerson, "Ocean surface wind speed measurements of the Special Sensor Microwave/Imager (SSM/I)," *IEEE Trans. Geosci. Remote Sensing*, vol. 28, pp. 823–828, 1990.
[29] J. Etcheto, Global Scale Validation of Wentz "Algorithms for retrieving wind speed and sea surface temperature from the SEASAT SMMR," Internal Rep. 90/02, Laboratoire d'Oceanographie Dynamique et de Climatologie (LODYC), 1990.
[30] F. Wentz, L. Mattox, and S. Peteherych, "New algorithms for microwave measurements of ocean winds: applications to SEASAT and the Special Sensor Microwave Imager," *J. Geophys. Res.*, vol. 91, pp. 2289–2307, 1986.

Jouni T. Pulliainen was born in Imatra, Finland, in 1964. He received the M.Sc. degree and the Licentiate in Technology degree from the Helsinki University of Technology, Faculty of Electrical Engineering, in 1988 and 1991, respectively.

He is a research scientist in the Helsinki University of Technology, Laboratory of Space Technology. His research interests include microwave remote sensing applications and technology. Recently, his work has been emphasized on the active remote sensing of forests.

Juha-Petri Kärnä was born in Helsinki, Finland, in 1965. He received the M.Sc. degree from the Helsinki University of Technology, Faculty of Electrical Engineering, in 1990.

He is currently a research scientist with the Technical Research Centre of Finland, Instrument Laboratory, Section for Remote Sensing. His research interests include microwave remote sensing, analysis of remotely sensed images and software engineering.

Martti Hallikainen (M'83-SM'85-F'93), for a photograph and biography, please see page 168 of this issue of the TRANSACTIONS.